Submitted to JGR-Solid Earth September 10, 2005

#2005JB004037

Stimulated Thermal IR Emission from Rocks: Assessing a Stress Indicator

Friedemann T. Freund[1,2], Akihiro Takeuchi[2,3], Bobby W.S. Lau[2], Akthem Al-Manaseer[4], Chung C. Fu[5], Nevin A. Bryant[6], and Dimitar Ouzounov[7]

[1] Ecosystems Science and Technology Branch, Code SGE, NASA Ames Research Center, Moffett Field, CA 94035-1000; +1-650-604-5183, ffreund@mail.arc.nasa.gov

[2] Department of Physics, San Jose State University, San Jose, CA 95192-0106, +1-408-386-8815, blau@science.sjsu.edu

[3] Department of Chemistry, Niigata University, Ikarashi-ninotyo, Niigata 950-2181, Japan +81-25-262-6169, takeuchi@curie.sc.niigata-u.ac.jp

[4] Department of Civil Engineering, San Jose State University, San Jose, CA 95192-0083 +1-408-924-3860, akthem@email.sjsu.edu

[5] Department of Civil Engineering, University of Maryland, College Park, MD 20742 +1-301-405-2011, ccfu@eng.umd.edu

[6] Jet Propulsion Laboratory, Org. 3880, Pasadena, CA 91109-8099 +1-818-354-7236, Nevin.A.Bryant@jpl.nasa.gov

[7] CEORS, George Mason University, Fairfax, VA 22030-4444 +1-301-614-6498, d.ouzounov@erols.com

Abstract

We report on the thermal infrared (TIR) radiation emitted from the surface of anorthosite. Using a BOMEN FT-IR spectroradiometer we measured the emission over the 800-1300 cm^{-1} (7.7-12.5 μm) range from the front face of a 60 x 30 x 7.5 cm^3 block of anorthosite during uniaxial stressing ~40 cm from the emitting rock surface. Stress is known to activate electronic charge carriers, i.e. defect electrons in the oxygen anion sublattice, known as positive holes or p-holes for short, which can spread through unstressed rock. Upon loading, the emission intensity changes near-instantly, reaching 150 mK. Narrow bands appear in the 800-950 cm^{-1} (10.5-12.5 μm) window, centered at 930 cm^{-1} (10.75 μm), 880 cm^{-1} (11.36 μm), and 820 cm^{-1} (12.4 μm). These bands are consistent with O-O stretching modes due to recombination of p-holes forming vibrationally excited O-O bonds that de-excite radiatively. Additional narrow bands occur in the 1000-1300 cm^{-1} (10.0-7.7 μm) range. The emitted intensity is lowest near 1150 cm^{-1} and 1030 cm^{-1} (8.7 and 9.7μm) where anorthosite has its strongest 300 K emission bands. The observed changes in the TIR spectrum and intensity cannot be due to frictional heat reaching the emitting surface, but rather point to p-holes spreading out from the stressed rock volume into the unstressed rock, reaching the surface, recombining, and leading to stimulated TIR emission due to hole-hole recombination luminescence. This process may lead to a better understanding of pre-earthquake TIR anomalies observed in night-time satellite images, also referred to as "thermal anomalies".

I Introduction

The Earth receives energy from the Sun in the form of solar radiation in the visible range (380-625 nm) and emits back longer wavelength radiation in the thermal infrared region (TIR). Since the late 1980s and early 1990s non-stationary TIR anomalies have been identified in night-time satellite images over land surface areas that seemed to be linked to active faults and impending earthquake activity [*Gornyi, et al*., 1988; *Qiang, et al*., 1991; *Qiang, et al*., 1990; *Srivastav, et al*., 1997]. TIR fluctuations equivalent to 2-4°C have been reported using from polar orbit and geostationary satellites. The cause of these apparent surface temperature excursions, often called "thermal anomalies" has remained enigmatic [*Cui, et al.*, 1999; *Srivastav, et al*., 1997; *Tronin*, 2000; *Tronin*, 2002; *Tronin, et al*., 2004].

Any explanation of TIR anomalies has to account for the face that, prior to major California earthquakes, no subsurface temperature increase has been observed in boreholes [*Johnston and Linde*, 2002] to within ±1 mK [*M.J.S. Johnston, private communication, Dec. 2004*]. The lack of subsurface temperature variations rules out that the TIR anomalies are caused by sensible heat flowing upward from below. Several other processes have been considered: (i) rising fluids that could lead to the emanation of warm gases [Gorny et al., 1998]; (ii) rising well water levels and changing moisture content in the soil [*Chadha, et al.*, 2003]; (iii) diffuse CO_2 emanation, leading to a "local greenhouse" effect [*Quing, et al.*, 1991; *Tronin*, 1999; *Tronin*, 2002]; and (iv) Near-surface air ionization due to enhanced radon emission and latent heat changes due to changes in the air humidity [*Pulinets, et al.*, 2005]. However, no comprehensive explanation has yet been proposed that would be acceptable to the science community .

Non-Conventional Approach

Recognizing the difficulties in finding an explanation using conventional (macroscopic) processes, we approach the TIR anomalies from a non-conventional (microscopic) perspective. We begin from the premise that the TIR phenomenon is linked to or the consequence of tectonic stresses building up in the rocks that underlie the areas with the apparent temperature excursions. We combine this statement with the recent discovery of highly mobile charge carriers, which are activated in rocks by the application of stress [*Freund*, 2002; *Freund, et al.*, 2004a]. Rocks in which such charge carriers appear include quartz-bearing granite, and quartz-free anorthosite and gabbro. The charge carriers are electronic, consisting of defect electrons in the oxygen anion sublattice. As such they represent holes in the valence band of otherwise insulating minerals. These charge carriers are known as positive holes or p-holes for short. They are unusual in as much as they are able to propagate fast and with apparently little attenuation through unstressed rocks over distances on the order of meters in laboratory experiments.

Next we demonstrate the special properties of p-holes. **Figure 1a** shows the principal stress, expressed in the deformed shape as obtained by finite element analysis, of a rectangular 1.2 m long slab of air-dry granite with a 10 x 15 cm^2 cross section. The slab was fitted with electrodes at both ends as indicated in **Figure 1b** to measure the currents flowing out of the stressed rock volume and a capacitive sensor to detect changes in the surface potential. The slab was electrically insulated from the pistons and at one end was placed under uniaxial compression loading it at 6 MPa/min to 67 MPa, about 1/3 failure strength. Loading and unloading was repeated 6 times.

As shown in **Figure 2**, when we apply stress, we instantly observe two currents flowing out of the slab. The currents are self-generated, i.e. they flow without externally applied voltage. One

current (shown in blue) is carried by electrons, the other (shown in red) is carried by holes. The currents are of the same magnitude and obviously flow out of the stressed rock volume in opposite directions. They increase with increasing stress but also fluctuate. The fluctuations are synchronous. Sometimes, as in the case presented in **Figure 2**, fluctuations are relatively small. At other times, with other geometries, they reach large amplitudes. In the case of the granite slab, the currents flowing out of ≈1500 cm^3 reach +7 nA and -7 nA at the maximum load, 67 MPa, which corresponds to ~1/3 the failure strength. Other igneous rocks such as the anorthosite and gabbro can generate even larger currents per unit volume rock, larger by a factor of 10-50. When we hold the stress constant, the outflow currents continue for hours with little attenuation suggesting that, once activated, the charge carriers have very long lifetimes. We also conducted experiments with wet rocks, applying two Cu electrodes to the unstressed end of a rock, one in direct contact with the rock surface, the other immersed in a 3 mm deep, 2 cm wide and 12 cm long pool of water. Alternating between the two electrodes we can demonstrate that the hole current, which flows through the unstressed rock, is able to pass through 1 cm water. A detailed account will be given elsewhere [*Freund, et al*., 2005].

The flow of the two currents is clearly activated by the application of stress. Since no mobile charge carriers are apparent in the rock before application of stress, we conclude that the charge carriers pre-exist in the rock in an electrically inactive, dormant form. The stress "awakens" these dormant precursors and releases both electrons and holes[1].

Once p-holes are activated, they spread out and accumulate at the surface forming a positive surface charge layer [*King and Freund*, 1984]. This surface charge has been confirmed by

[1] Another method to activate the dormant precursors and generate p-hole charge carriers is by heating to temperatures above 400-450°C [Freund, F., et al. (1993), Critical review of electrical conductivity measurements and charge distribution analysis of magnesium oxide, *J. Geophys. Res*., *98*, 22209-22229, Freund, F. T. (2003), On the electrical conductivity structure of the stable continental crust, *J. Geodynamics*, *35*, 353-388.]

measuring the surface potential [*Freund, et al.*, 1993; *Freund*, 2003]. **Figure 3** shows the build-up of the surface potential as recorded by the capacitive sensor on the top of the granite slab (see **Figure 2**). The surface potential is positive and increases by +25 mV as the stress increases. If surface potentials are measured under open circuit conditions, i.e. without drawing currents out of the rock, they reach values of +1.4 to +1.75 V [*Takeuchi and Nagahama*, 2002a]. When cracks occur, short positive voltage pulses in the 10-20 V range have been observed [*Freund, et al.*, 2004a]. Next we sought to study whether the arrival of p-hole charge carriers at the rock surface might lead to recognizable changes in the TIR emission characteristics.

Experimental Part

We chose anorthosite, an essentially monomineralic feldspar rock, composed of the Ca-rich plagioclase labradorite. Our sample, available under the trade name "Blue Pearl", came from Larvik, Norway, a very coarse-grained anorthosite with crystals in the size range of 20-40 mm, a density of 2.7 g/cm^3, and a compressive strength of 181-187 MPa.

We uniaxially stressed the air-dry anorthosite block, 60 x 30 x 7.5 cm^3, via a pair of pistons (11.25 cm diameter). The load was applied up to failure off-center as sketched in **Figure 4a**. The off-center loading concentrated the stresses away from the TIR emitting surface. **Figure 4b** displays the principal stress as obtained by finite element analysis. The front part, in particular the emitting surface, remained essentially stress-free.

The pistons were electrically insulated from the rock through 0.8 mm thick sheets of high density polyethylene with a resistivity of $>10^{14}$ Ω cm. The load was applied at a constant stress rate of 6.3 MPa/min up to failure, using a hydraulic 225 ton SATEC press, model RD 2000kN.

Emission spectra were recorded from a circular area, 5 cm diameter, off the front surface of the rock, flat but rough as cut with the diamond saw. We used a Bomen MB-100 FT-IR spectroradiometer equipped with a Peltier-cooled HgCdTe detector and two integrated blackbody emitters for internal calibration, one at ambient temperature, the other at 60°C, plus a computer-controlled switching mirror to collect the IR radiation sequentially from the sample and the two blackbody emitters. The space between the rock and the spectrometer, about 1 m, was shielded from ambient light. The room was semi-darkened. During the measurement the movement of people was restricted to avoid any changes in the reflected IR radiation field.

The spectra were recorded over the wavenumber range 700-1400 cm^{-1} (7.14–14.25 μm) at 2 cm^{-1} resolution. Each FT-IR file consists of 25 co-added scans from the rock surface plus 5 scans each from the ambient temperature and 60°C blackbody emitters. Each file took 40 sec to acquire and store. The radiometric noise at the single scan level was above 100 mK, improving to about 10 mK upon averaging 250 scans. The run lasted for a total of 36 min 40 sec, comprising 1375 scans. During the first 6 min 40 sec 10 pre-loading files were acquired. During the next 30 min, 35 additional files were acquired up to failure. The energy emitted is given in blackbody temperature equivalents in units of degrees C, K or mK.

Results

Many studies of electromagnetic and other basic phenomena accompanying rock fracture have been carried out under conditions emulating the procedures prescribed by ASTM C170-50 and DIN 52102, i.e. with cylindrical test samples to be loaded over their entire cross section [*Brady and Rowell*, 1986; *Lockner*, 1993; *Rowell, et al.*, 1981; *Warwick, et al.*, 1982; *Yoshida and Ogawa*, 2004]. Loading over the entire cylinder cross section causes the surface to bulge

outward, normal to the applied stress, leading to tensile stresses in the surface layer, which in turn lead to microfracturing. Microfracturing causes fracto- and triboluminescence and has been shown to contribute to the emission of visible and IR radiation [*Brady and Rowell*, 1986].

By applying stress to only a small portion of a large block, we simulates more accurately what happens in the Earth before earthquakes. The rocks surrounding the stressed volume act as pressure confinement and absorb much of the compressive stresses that result from the outward bulging of the stressed volume. As the stresses rise, mineral grains in the stressed volume and the immediate surrounding begin to deform plastically. By loading the rock off-center as shown in **Figure 4a/b**, the tensile stresses only affect the back portion. As a result the front face, from where the IR radiation was recorded, remained essentially stress-free throughout the experiment.

Figure 5 shows the TIR emission spectrum from 800 to 1300 cm^{-1} (7.7-12.5 mm) averaged from the 10 pre-loading files. The intensity scale is given in degree Celsius relative to a blackbody emitter. The maxima of the emitted intensity around 1020 cm^{-1} and 1190 cm^{-1} (9.8 mm and 8.4 mm respectively) with a smaller band around 1110 cm^{-1} (9.0 mm) are characteristic of thermally activated Si–O and Al–O stretching modes of labradorite [*Johnson, et al.*, 2002].

Figure 6a shows a 3-D plot of the intensity variations over the 7.4-14.3 μm range (700 to 1350 cm^{-1}), as a function of time while 46 files were acquired, 40 sec each, 10 files before and 36 files during loading up to failure of the rock. The energy of the emitted IR radiation is given in degree Kelvin. During the first 400 sec, while we acquire the 10 pre-load files, the intensity is constant indicating that the ambient temperature was stable. In the instant the load is applied the emission spectrum changes. Some emission bands increase in intensity and new bands appear.

The intensity of the IR emission fluctuates as the load increases. Such fluctuations have been observed during every IR emission experiment carried out so far. They resemble the fluctuations

of the outflow currents mentioned in the context of **Figure 2**. They are not an experimental artifact but an inherent feature of the processes inside the rock that lead on one hand to outflow currents and an the other hand to the changes in IR emission as exemplified in Figure 6a.

To obtain **Figure 6b** we subtracted the average of the pre-load files from each of the files acquired during loading. The intensity scale is given in mK. There are three prominent features:

(i) The difference spectra bring out more clearly the narrow emission bands at the beginning of loading. Three bands can be identified between 800-950 cm^{-1} (10.5-12.5 μm) together with similar bands at higher wavenumbers (shorter wavelengths).

(ii) The difference spectra amplify the intensity fluctuations, which are synchronous over the spectral range presented here, while the relative intensities shift over different spectral ranges.

(iii) The difference spectra show that the maximum of the excess intensity emitted during loading, in particular close to failure, does not coincide with the maximum of the pre-load emission spectrum. On the contrary, the excess intensity emitted in the 1000-1100 cm^{-1} window, which includes the pre-load emission maximum at 9.7 μm, is conspicuously low during loading.

This last point is highlighted in **Figure 7** where we plot the integrated excess TIR emission intensity versus wavenumbers during loading up to failure. For comparison we also show the pre-load spectrum. There are two maxima in the pre-load emission spectrum at 1080 cm^{-1} and 1210 cm-1 (9.7 and 8.5 μm), but the integrated excess emission intensity exhibits two minima close to these values plus several narrow maxima in the 800-950 cm^{-1} (10.5-12.5 μm) region.

Discussion

Sensible heat flow from a stressed rock volume that is 40 cm from the emitting rock surface cannot account for the near-instantaneous change in the spectrum and intensity of the IR emission from the front face of the anorthosite block as reported in **Figure 6a/b**. The changes are too fast to allow for frictional heat to flow from the stressed rock to the emitting surface by heat diffusion. This leads us to conclude that a process other than sensible heat flow must be responsible for the observed changes in the TIR emission characteristic.

Impact experiments have shown that the application of sudden stress activates electronic charge carriers [*Freund*, 2002]. These charge carriers are defect electrons in the O^{2-} sublattice, chemically O^{-} in a matrix of O^{2-}, equivalent to "holes" in the valence band, also known as positive holes or p-holes for short. They normally lie dormant in the form of positive hole pairs, PHPs, which – in chemical terms – consist of peroxy anions, O_2^{2-}, in oxide materials like MgO [*Freund, et al.*, 1993] or peroxy linkages in silica and silicate minerals, $O_3X/^{OO}\backslash XO_3$ with X = Si^{4+}, Al^{3+} etc. [*Freund*, 2003; *Ricci, et al.*, 2001]. Application of stress causes the PHPs to break and to release p-hole charge carriers. The charge cloud carried by p-holes can propagate at relatively high speed through the rock, 100-300 m sec^{-1}, consistent with a phonon-assisted electron hopping mechanism [*Freund*, 2002].

The near-instantaneous changes in the infrared emission characteristics described here point to p-holes that arrive at the rock surface as the most likely agents. To further characterize this process we need to know (i) how PHPs are activated by stress, (ii) how p-hole charge carriers propagate through unstressed rock, and (iii) what happens when p-holes arrive at the surface.

(i). When a rock is subjected to mechanical stress, deformations occur first at microscopic points, where stresses concentrate along grain-grain contacts, later throughout the volume. With

stresses increasing, existing dislocations begin to move or new ones are generated. Dislocation movement is the dominant deformation mechanism in metals and ductile materials [*Miguel, et al*., 2001], but also occurs in brittle materials where, under stress, dislocations tend to collapse into shear planes, which in turn initiate microfracturing [*Moore and Lockner*, 1995; *Ohnaka*, 1995]. The important point in the context of this paper is that, when a moving dislocation intersects a peroxy link, it breaks the O^--O^- bond. The breakage involves energy levels of the O-O bond that are normally unoccupied. As described in detail elsewhere [*Freund, et al*., 2005] the unoccupied level is strongly antibonding, i.e. its associated wavefunction points away from the O-O bond. When a moving dislocation disturbs this O-O bond this unoccupied level shifts downward, allowing an electron from a neighboring O^{2-} to hop in. Hopping in of an electron is equivalent to a hole hopping out, thereby creating a p-hole charge carrier.

(ii) The p-holes are highly mobile. They propagate as an electronic charge, without atomic diffusion, through the valence band. Their wavefront can travel fast, on the order of 100-300 m/sec. They spread out from the rock volume, in which they are generated, into the surrounding unstressed rock [*Freund*, 2002]. In addition, being the only mobile charge carriers in an otherwise insulating medium, p-holes spread to the surface forming a surface charge layer [*King and Freund*, 1984]. This process can be followed by measuring surface potentials [*Freund, et al.*, 1993]. Typical surface potential values measured under open circuit conditions are +1.5 V to +1.75 V corresponding to surface charge densities on the order of 10^{-5} Coulomb/m^2 or 10^{13}-10^{14} p-holes/m^2 [*Takeuchi, et al*., 2005; *Takeuchi and Nagahama*, 2002b].

(iii) The energy required to break a peroxy bond can be estimated from measurements of the electrical conductivity as a function of temperature. In one well-characterized case pertaining to peroxy in MgO [*Freund, et al.*, 1993], the activation energy was estimated to be 2.4 eV [*Freund,*

et al., 1993; *Freund*, 2003]. Similar activation energies are expected to apply to peroxy links in silicate minerals and, by extension, in rocks.

If it costs energy to generate p-holes, energy will be regained when p-holes recombine. The recombination of p-holes is hampered by the fact that they are positively charged. Their electrostatic repulsion is probably responsible for the long lifetimes p-hole and for the fact that p-holes do not readily recombine inside the rock volume. However, the surface is a special place where p-holes achieve higher number densities than in the bulk [*King and Freund*, 1984]. Higher densities mean higher probabilities for recombination.

Figure 8 conceptualizes the process when two p-holes arrive at the surface and settle on two adjacent oxygen anions. The surface is represented by three corner-linked SiO_4 tetrahedra, two of which terminate at the surface with non-bonded oxygens. Two curved arrows in the left panel symbolize the path the two p-holes, which change two surface oxygens from O^{2-} to O^{-}. The right panel indicates that the two O^{-}recombine, snapping together to form the very short (1.5 Å) O^{-}–O^{-} bond characteristic of the peroxy link or PHP [*Ricci, et al*., 2001].

The energy released during p-hole recombination will be deposited into the newly formed O-O link, meaning that the O-O bond will be "born" in a vibrationally highly excited state. It can dissipate its excess energy: (i) by emitting photons at the characteristic energies of the O-O vibrational manifold or (ii) by channeling energy into neighboring Si-O and Al-O bonds, which in turn become vibrationally excited and emit at their characteristic frequencies. This stimulated TIR emission represents a hole-hole IR luminescence. It bears resemblance to the electron-hole recombination in semiconductors that provides the physical basis for light-emitting diodes (LED). The main difference is that, in the case of hole-hole recombination, electrostatic repulsion prevents p-holes from recombining until they come together to close that attraction takes over allowing two p-holes to gain energy by reconstituing the O–O bond.

We use this concept to estimate how much energy can be radiated off a rock surface where p-hole recombination takes place. For surfaces in thermodynamic equilibrium at 300 K the emission spectrum such as shown in **Figure 5** consists of bands that arise from downward transitions from quantum levels $n_i \geq 1$, which become populated at the mean thermal energy $kT_{300K} \approx 25$ meV. We are interested in the TIR region around 1000 cm^{-1} or 10 μm, corresponding to energy levels separated by ≈100 meV. The probability to thermally populate a level E_n is given by a Boltzmann distribution, $\exp[-E_n/kT]$. With $kT_{300K} \approx 25$ meV, the probability to populate the first excited level 100 meV above the ground level n=0, is $e^{-4} \approx 2 \times 10^{-2}$ or ≈2 %. To populate the second excited state, n=2, at ≈200 meV the probability drops to $e^{-8} \approx 10^{-4}$ or ≈0.02 %. To populate the n=3 and higher levels the probability drops rapidly. Therefore, in case of the TIR emission in the 10-12 μm window, levels above n=1 are sparsely populated at 300 K and nearly all intensity emitted is due to downward transitions from n=1 to n=0 levels. Emission bands due to downward transitions involving levels with $n \geq 1$ are called "hot bands", because they reflect transitions between vibrationally "hot" states. Hot bands in the 1000 cm^{-1} or 10 μm region are too weak to be observed at 300 K.

The difference spectra in **Figure 6b** show a series of narrow emission bands, especially at the start of loading. The bands at 930 cm^{-1} (10.75 μm), 870 cm^{-1} (11.5 μm), and 810 cm^{-1} (12.35 μm) are consistent with the transition energies between vibrationally excited levels of O-O bonds. For the peroxy link $O_3Si/^{OO}\backslash SiO_3$ in SiO_2 the energy of the fundamental O-O stretching mode, i.e. for the transition n=1 to n=0, is known to be 920-930 cm^{-1} (10.75-10.87 μm) [*Ricci, et al.*, 2001]. The energies for the O-O "hot band" transitions from n=2 to n=1 and from n=3 to n=2 are not known, but they must lie at slightly lower wavenumbers. An energy difference of ~60 cm^{-1} is reasonable. Hence, we tentatively assign the bands at 870 cm^{-1} (11.5 μm) and 810 cm^{-1} (12.35 μm) to the first and second hot bands of the O-O bond, corresponding to n=2 to n=1 and n=3 to

n=2 transitions respectively. **Figure 6b** shows additional narrow bands at higher wavenumbers (shorter wavelength) in the 1000-1200 cm^{-1} (8.3-10 μm) range. We tentatively assign these bands to transitions where the O-O stretching mode combines with low-frequency lattice modes.

The intensity evolution of the suspected O-O bands at 930 cm^{-1} (10.75 μm), 870 cm^{-1} (11.5 μm), and 810 cm^{-1} (12.35 μm) is replotted in **Figure 9** for three 2 minute time intervals after beginning of loading. The bands at 810 cm^{-1} (12.35 μm) and 870 cm^{-1} (11.5 μm), which we assign to hot transitions, exhibit higher intensities in the beginning. Later the fundamental at 930 cm^{-1} (10.75 μm) gains intensity, while the hot bands loose their narrow character.

The narrow bands in the 1000-1200 cm^{-1} (8.3-10 μm) range in **Figure 6b** display a similar intensity evolution as a function of time. This is consistent with the concept drawing in **Figure 8** where we indicate on the right side that the vibrationally highly excited O-O bond will "kick" its neighbors and excite their vibrational modes. As seen in **Figure 7** the total excess intensity emitted over the course of the loading experiments shows pronounced maxima at 1150 and around 1300 cm^{-1} (8.7 and ≈7.7 μm respectively), which suggest transitions of the O-O stretching modes jointly with lattice modes in the 250 and ≈400 cm^{-1} (40 μm and ≈25 μm) regions.

By contrast, the minima in the total excess intensity curve in **Figure 7** suggest that the usual lattice modes of anorthosite do not become excited, or less excited, when p-holes recombine. This implies that, while much of the vibrational excess energy of the newly formed O-O bonds is radiated away in discrete TIR photons at 930 cm^{-1} (10.75 μm), 870 cm^{-1} (11.5 μm), and 810 cm^{-1} (12.35 μm) or used to excite discrete lattice modes in the 250 and 400 cm^{-1} (40 μm and ≈25 μm) windows. In other words, the surface does not really gets heated. Therefore, the fact that the 300 K emission maxima lie close to the minima in the integrated excess intensity curve supports the idea of a non-thermal TIR luminescence due to hole-hole recombination as proposed here.

We can use these data to also estimate how many p-hole recombination events are needed to produce a 150 mK increase of the radiation temperature relative to a blackbody emitter. As mentioned above, the activation energy for breaking peroxy bonds and generating p-holes has been estimated to be 2.4 eV [*Freund*, 2003]. In units of kT, the thermal energy (where k is the Boltzmann constant) 2.4 eV correspond to ~28,000 K. If, at the upper limit, 2.4 eV are regained during p-hole recombination, $\sim 10^5$ p-hole recombination events would be needed to raise the temperature by 150 mK. Our emitting surface area is $\approx$20 cm^2 containing a total of $\approx 2 \times 10^{16}$ oxygen anions in the top surface layer. We also know that, in order to produce a surface potential of +1 V, approximately 10^{10} p-holes have to come to the 20 cm^2 surface area from which we measure the TIR emission, equivalent to $\sim 10^{-5}$ Coulomb m^{-2}, equivalent to $\sim 10^{13}$ m^{-2} [*Takeuchi and Nagahama*, 2002b]. Therefore, $\sim 10^{10}$ p-holes are expected to become available in the 5 cm diameter surface area from which we measure the TIR emission, equal to ~20 cm^2. Of those 10^{10} p-holes only a very small fraction, 2×10^5, need to recombine in the manner discussed above. .

This order-of-magnitude estimate shows that, within the uncertainties of our TIR emission experiment, the observed excess radiated TIR emission can be accounted for by p-holes in the surface charge layer recombining and emitting their excess energy. Therefore, a radiative p-hole recombination at the rock surface as the cause for the observed excess TIR intensity appears to be physically plausible.

Lastly, we address the recurring observation that the emitted IR intensity always fluctuates as we increase the stress [*Ouzounov and Freund*, 2004]. During rock deformation experiments we see similar fluctuations in the two electric currents that flow out of the stressed rock volume in opposite directions, one carried by electrons, the other by p-holes [*Freund, et al.*, 2005; *Freund,*

et al., 2004b]. The two currents are tightly coupled via their respective electric fields. This, in turn, causes the fluctuations. With this background knowledge we can state with some degree of certainty that the observed intensity fluctuations of the emitted TIR radiation are not an artifact. They are part of a pattern of the p-hole currents that flow out of the stressed rock volume. If the enhanced TIR emission from the rock surface is caused by p-holes that reach the surface and radiatively recombine as we surmise here, any fluctuations in the number of p-holes arriving at the surface will be reflected in intensity variations of the TIR emission.

It is too early to say to what extent the findings described here can be applied to geophysical scenarios where stresses build up deep in the Earth's crust prior to major earthquakes. To produce TIR anomalies, which can be recorded by satellites, p-holes activated at depth would have to reach the Earth's surface. Experimentally we have demonstrated that p-holes can spread and propagate through more than a meter of dry granite and over similar distances through other igneous rocks [*Freund, et al*., 2005]. We know that p-holes, once activated, have lifetimes of the order of many hours to days. We also know that even a 1 cm thick layer of water does not "kill" the flow of p-hole charge carriers, though the presence of water modifies the flow pattern in ways that we only begin to understand.

Conclusions

The discovery of dormant electronic charge carriers in igneous rocks, which can be activated by stress, has potentially far-reaching consequences for understanding pre-earthquake signals and, in particular, pre-earthquake TIR anomalies identified in satellite images. The charge carriers are defect electrons in the valence band of the otherwise insulating silicate minerals, also known as positive holes or p-holes for short. Once activated, p-holes are able to spread through rocks. At the rock surface they recombine. Because energy is released during recombination,

vibrationally excited states of O-O bonds form. The radiative de-excitation of the O-O bonds leads to characteristic changes in the TIR emission marked by the appearance of narrow bands in the 800-950 cm^{-1} (10.5-12.5 μm) range. These diagnostically distince emission bands point at hole-hole recombination luminescence as the underlying physical process.

Acknowledgements

This work would not have been possible without support from Zhengming Wan and his coworkers Yulin Zhang and Qincheng Zhang, ICESS, University of California at Santa Barbara, who brought their BOMEN radiospectrometer and other radiometric equipment three times to our laboratory. They helped us record the emission spectra but do not necessarily accept our interpretation of the results. We thank Yingwei Fei, Geophysical Laboratory, Carnegie Institution of Washington, and Murzy Jhabvala, NASA Goddard Space Flight Center, for encouraging the early phases of this project. We acknowledge financial support through grants from the NASA Ames Research Center Director's Discretionary Fund. B.W.S.L. is supported by a grant from the National Geospatial Agency (NGA). A.T. acknowledges support from the Japan Society for the Promotion of Science (JSPS) for Young Scientists.

References

Brady, B. T., and G. A. Rowell (1986), Laboratory investigation of the electrodynamics of rock fracture, *Nature*, *321*, 488-492.

Chadha, R. K., et al. (2003), Search for earthquake precursors in well water levels in a localized seismically active area of reservoir triggered earthquakes in India, *Geophy. Res. Lett.*, *30*, 69-71.

Cui, C., et al. (1999), Monitoring the thermal IR anomaly of Zhangbei earthquake precursor by satellite Remote sensing technique, paper presented at ACRS.

Freund, F. (2002), Charge generation and propagation in rocks, *J. Geodynamics*, *33*, 545-572.

Freund, F., et al. (1993), Critical review of electrical conductivity measurements and charge distribution analysis of magnesium oxide, *J. Geophys. Res.*, *98*, 22209-22229.

Freund, F. T. (2003), On the electrical conductivity structure of the stable continental crust, *J. Geodynamics*, *35*, 353-388.

Freund, F. T., et al. (2004a), Stress-induced changes in the electrical conductivity of igneous rocks and the generation of ground currents, *Terrestrial, Atmospheric and Oceanic Sciences (TAO)*, *15*, 437-468.

Freund, F. T., et al. (2005), Cracking the Code of Pre-Earthquake Low Frequency EM Emissions, *Phys. Chem. Earth.*, *in review*.

Freund, F. T., et al. (2004b), Positive holes and their role during the build-up of stress prior to the Chi-Chi earthquake, paper presented at International Conference in Commemoration of 5th Anniversary of the 1999 Chi-Chi Earthquake, Taiwan, Taipei, Taiwan.

Gornyi, V. I., et al. (1988), The Earth's outgoing IR radiation as an indicator of seismic activity, *Proc. Acad. Sci. USSR*, *301*, 67-69.

Johnson, J. R., et al. (2002), Thermal infrared spectroscopy of experimentally shocked anorthosite and pyroxenite: Implications for remote sensing of Mars, *J. Geophys, Res.*, *107*, 3-1.

Johnston, M. J. S., and A. T. Linde (2002), Implications of crustal strain during conventional, slow and silent earthquakes, in *International Handbook of Earthquake and Engineering Seismology*, edited, pp. 589-605, Academic Press.

King, B. V., and F. Freund (1984), Surface charges and subsurface space charge distribution in magnesium oxide containing dissolved traces of water., *Phys. Rev.*, *B 29*, 5814-5824.

Lockner, D. (1993), The role of acoustic emission in the study of rock fracture, *Int. J. Rock Mechanics & Minind Sci.*, *30*, 883-899.

Miguel, M. C., et al. (2001), Intermittent dislocation flow in viscoplastic deformation, *Nature*, *410*, 667-671.

Moore, D. E., and D. A. Lockner (1995), The role of microcracking in shear-fracture propagation in granite, *J. Struct. Geol.*, *17*, 95-114.

Ohnaka, M. (1995), A shear failure strength law of rock in the brittle-plastic transition regime, *Geophysical Research Letters*, *22*, 25-28.

Ouzounov, D., and F. T. Freund (2004), Mid-infrared emission prior to strong earthquakes analyzed by remote sensing data, *Adv. Space Res.*, *33*, 268-273.

Pulinets, S., et al. (2005), Thermal, atmospheric and ionospheric anomalies around the time of Colima M7.8 earthquake of January 21, 2003, *Annales Geophysicae*, *submitted*.

Qiang, Z.-J., et al. (1991), Thermal infrared anomaly - precursor of impending earthquakes, *Chinese Sci. Bull.*, *36*, 319-323.

Qiang, Z. J., et al. (1990), Abnormal infrared theraml of satellite-forewarning of earthquakes, *Chinese Sci. Bull.*, *35*, 1324-1327.

Quing, Z., et al. (1991), Thermal infrared anomaly- precursor of impending earthquakes, *Chinese Science Bulletin*, *36*, 319-323.

Ricci, D., et al. (2001), Modeling disorder in amorphous silica with embedded clusters: The peroxy bridge defect center, *Physical Review B*, *64*, 224104-224101 - 224104-224108.

Rowell, G. A., et al. (1981), Precursors of laboratory rock failure, in *Fracture Mechnanics for Ceramics, Rocks, and Concrete*, edited by S. W. Freiman and E. R. Fuller, pp. 196-220, ASTM, Philadelphia, PA.

Srivastav, S. K., et al. (1997), Satellite data reveals pre-earthquake thermal anomalies in Killari area, Maharashtra, *Current Science*, *72*, 880-884.

Takeuchi, A., et al. (2005), Current and surface potential induced by stress-activated positive holes in igneous rocks, *Phys. Chem. Earth*, *this issue*.

Takeuchi, A., and H. Nagahama (2002a), Interpretation of charging on fracture or frictional slip surface of rocks, *Phys. Earth Planet. Inter.*, *130*, 285-291.

Takeuchi, A., and H. Nagahama (2002b), Surface charging mechanism and scaling law related to earthquakes, *J. Atmospheric Electricity*, *22*, 183-190.

Tronin, A. A. (Ed.) (1999), *Satellite thermal survey application for earthquake prediction*, 717-746 pp., Terra Sci. Publ., Tokyo, Japan.

Tronin, A. A. (2000), Thermal satellite data for earthquake research, paper presented at IGARSS 2000; IEEE 2000 international geoscience and remote sensing symposium. Taking the pulse of the planet: the role of remote sensing in managing the environment, IEEE, Honolulu, HI.

Tronin, A. A. (2002), Atmosphere-lithosphere coupling: Thermal anomalies on the Earth surface in seismic process, in *Seismo-Electromagnetics: Lithosphere-Atmosphere-Ionosphere Coupling*, edited by M. Hayakawa and O. A. Molchanov, pp. 173-176, Terra Scientific Publ., Tokyo.

Tronin, A. A., et al. (2004), Thermal anomalies and well observations in Kamchatka, *International Journal of Remote Sensing*, *25*, 2649-2655.

Warwick, J. W., et al. (1982), Radio emission associated with rock fracture: Possible application to the great Chilean easthquake of May 22, 1960, *J. Geophys. Res.*, *87*, 2851-2859.

Yoshida, S., and T. Ogawa (2004), Electromagnetic emissions from dry and wet granite associated with acoustic emissions, *J. Geophys, Res.*, *109*, 10.1029/2004JB003092.

Figures

(a)

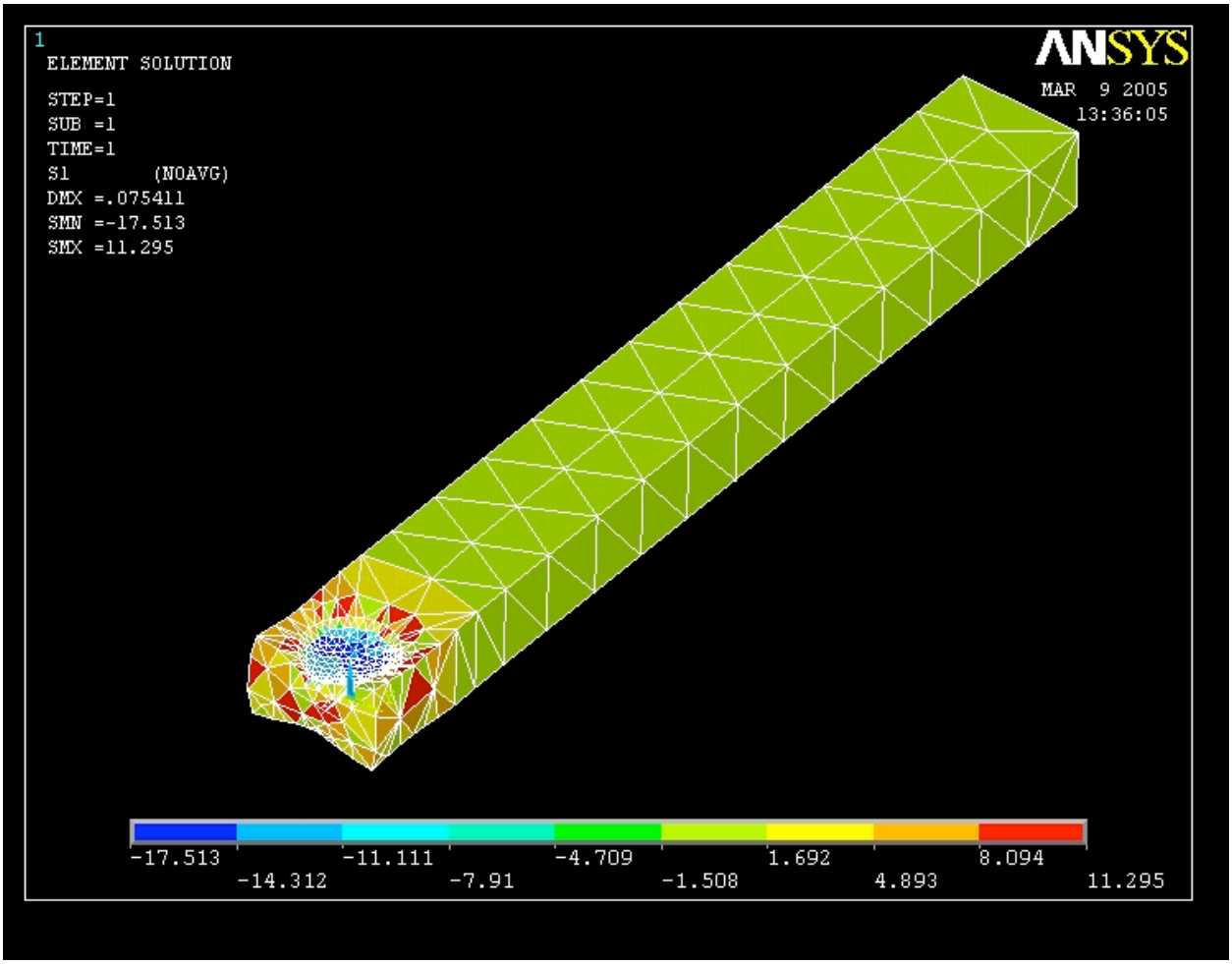

Figure 1 (a): Finite Element Analysis of the principal stress distribution in the granite slab loaded at one end to 1/3 failure strength.

(b)

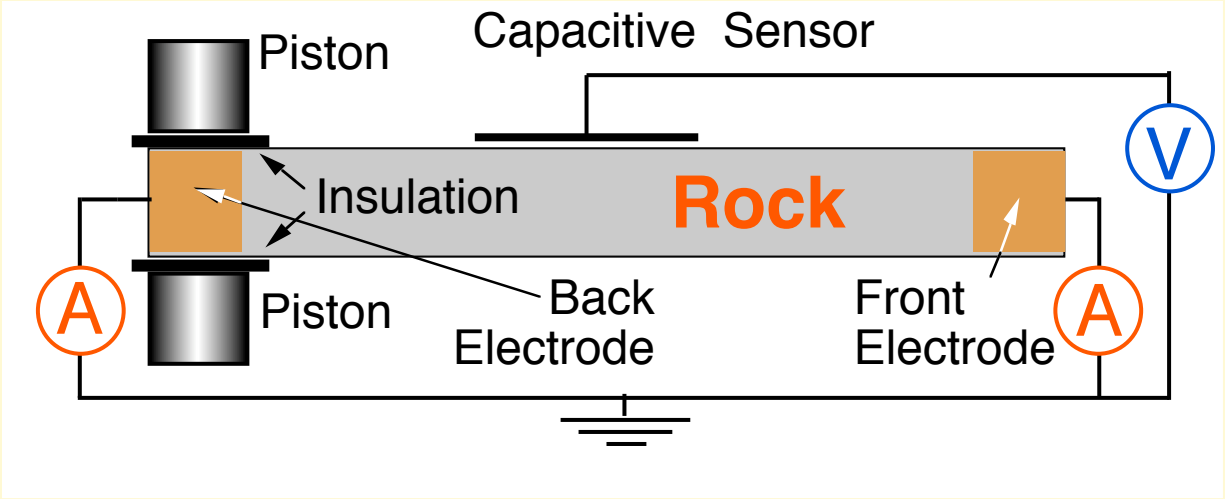

Figure 1 (b): Block diagram of the electric circuit for measuring the currents that flow out of the stressed rock without externally applied volts.

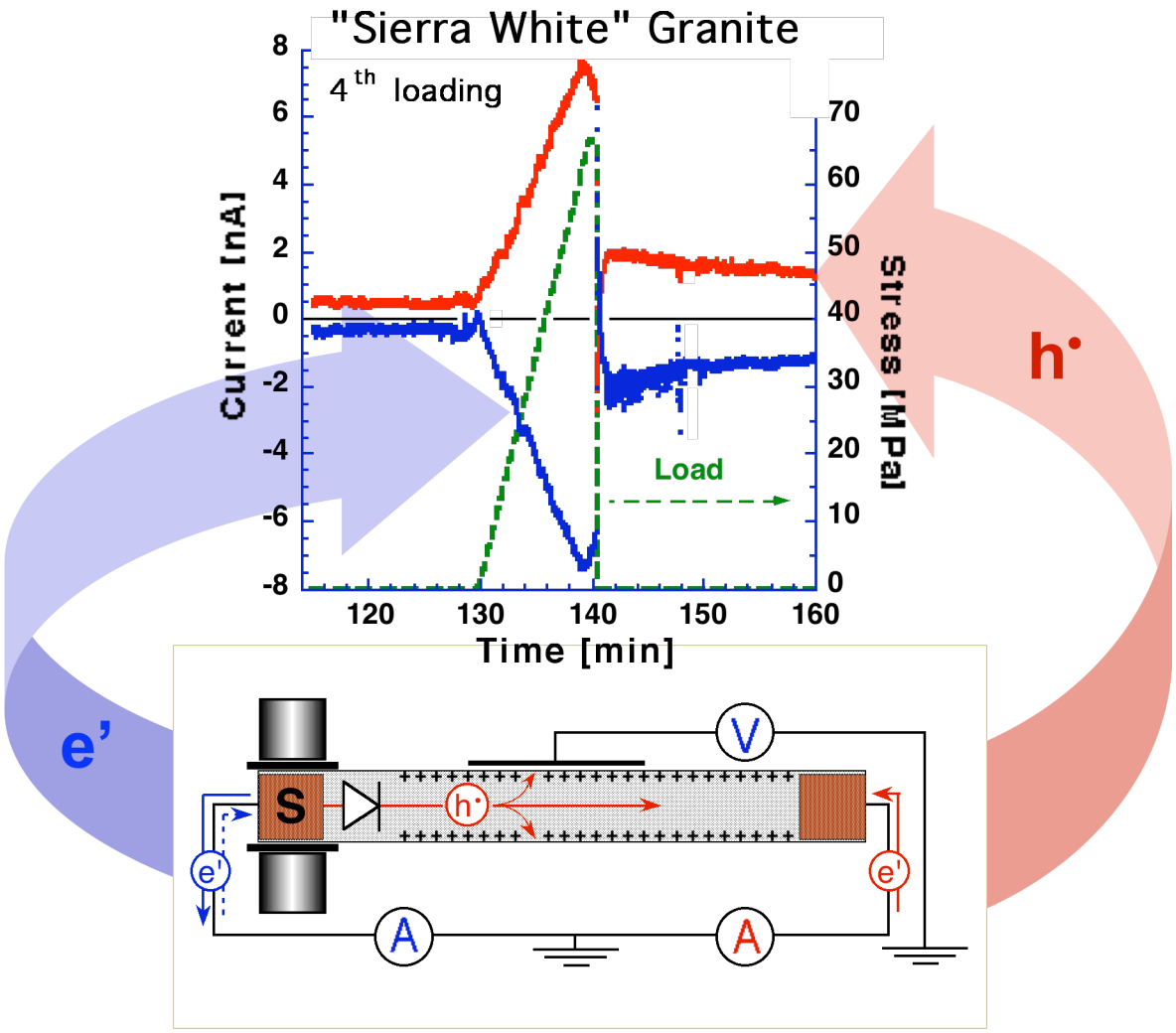

Figure 2: Two stress-activated currents flowing out of the stressed rock volume, the "source" S: an electron current flowing from the stressed rock volume into the electrode in direct contact with the rock under stress and a hole current flowing through the length of the slab, over 1 m or more of rock, into the electrode at the right end of the slab.

Below schematic representation of currents inside the rock and through the external circuit. The interface between stressed and unstressed rock acts as barrier for electrons.

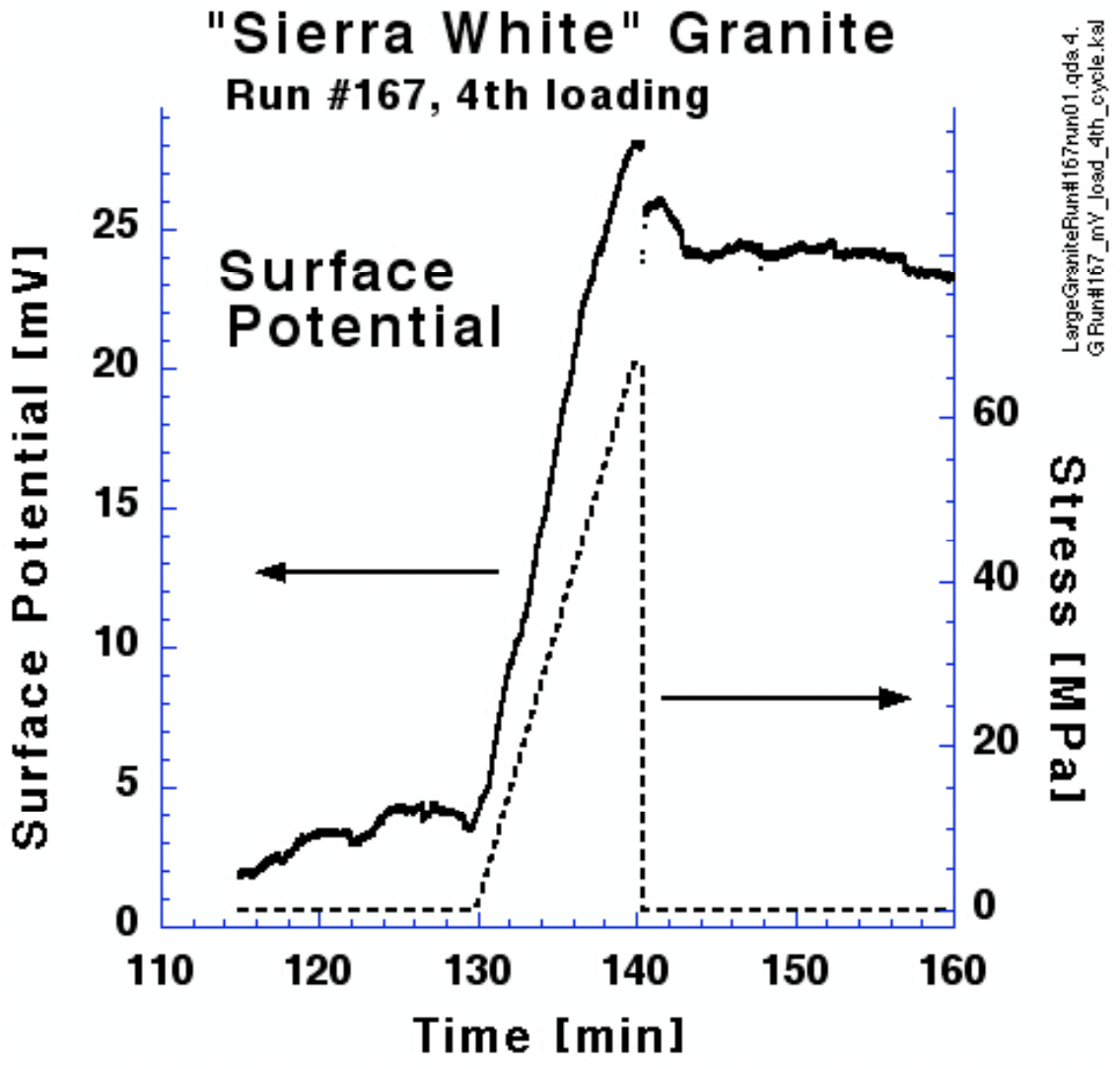

Figure 3*: Build-up of a positive surface potential measured with the capacitive sensor depicted in* ***Figure 1b*** *during loading one end of the 1.2 m long granite slab while currents are being drawn. Dotted line: Load profile.*

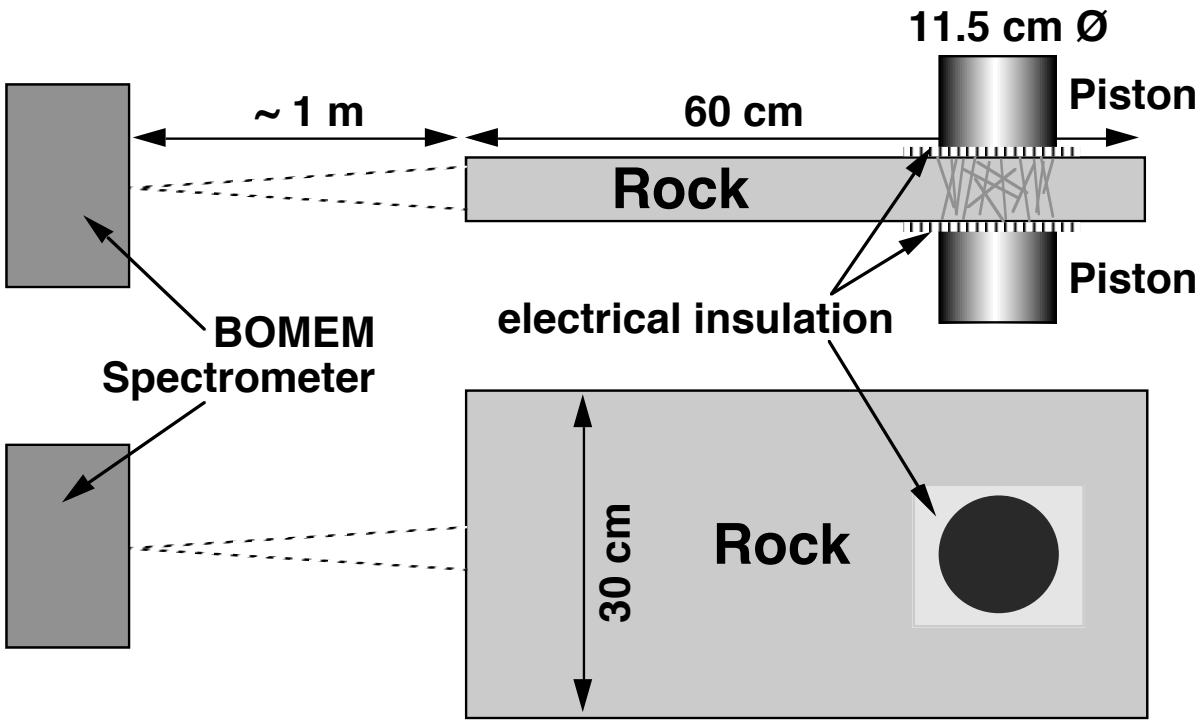

Figure 4a: Schematic of the set-up used to record the IR emission spectrum from the flat, saw-cut front face of a 60 x 30 x 7.5 cm^3 block of anorthosite during loading.

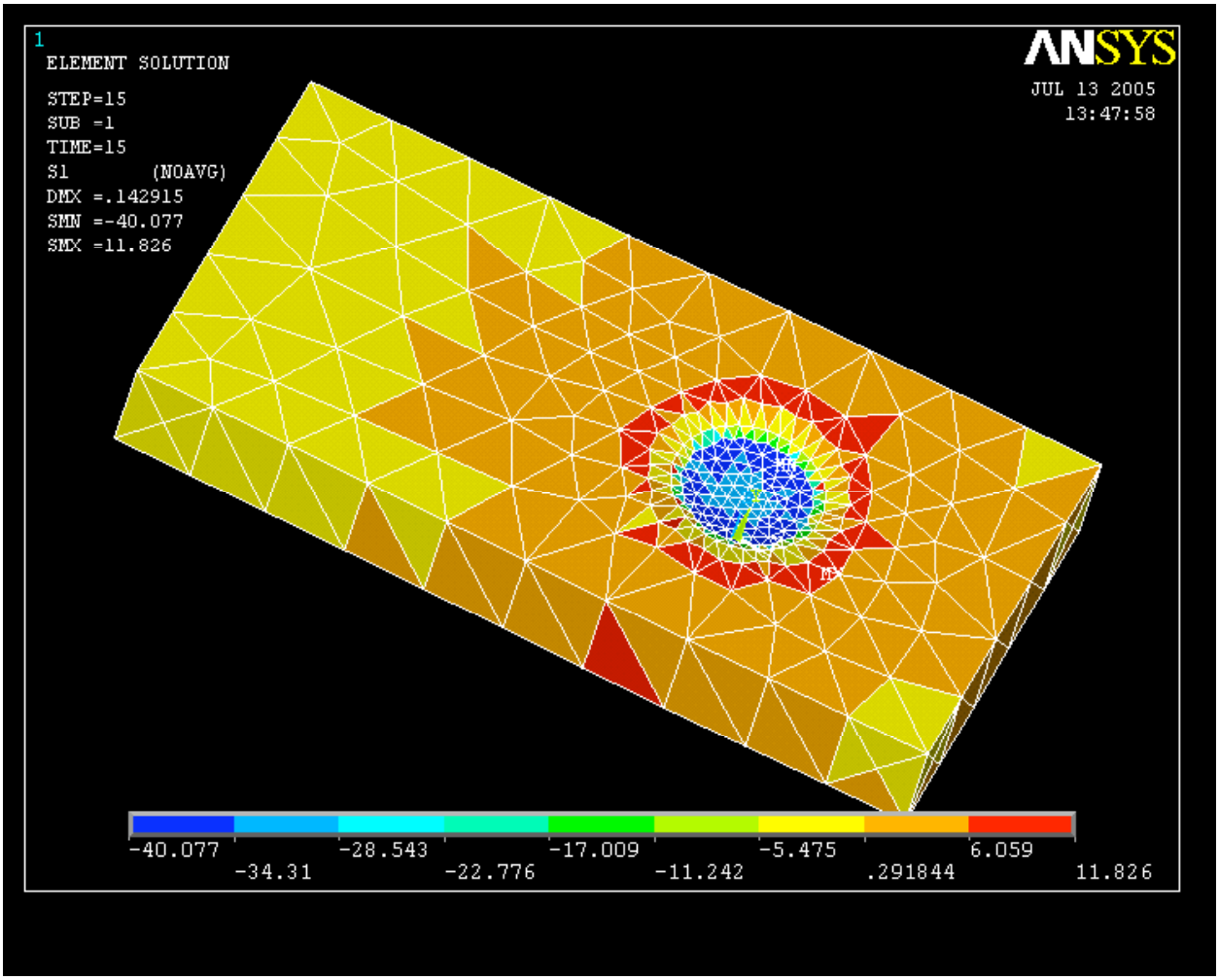

Figure 4b: Finite analysis representation, using a variable grid size, of the stress and strain distribution in the anorthosite block during asymmetric loading. The surface from which the IR emission is measured is the hidden surface on the right.

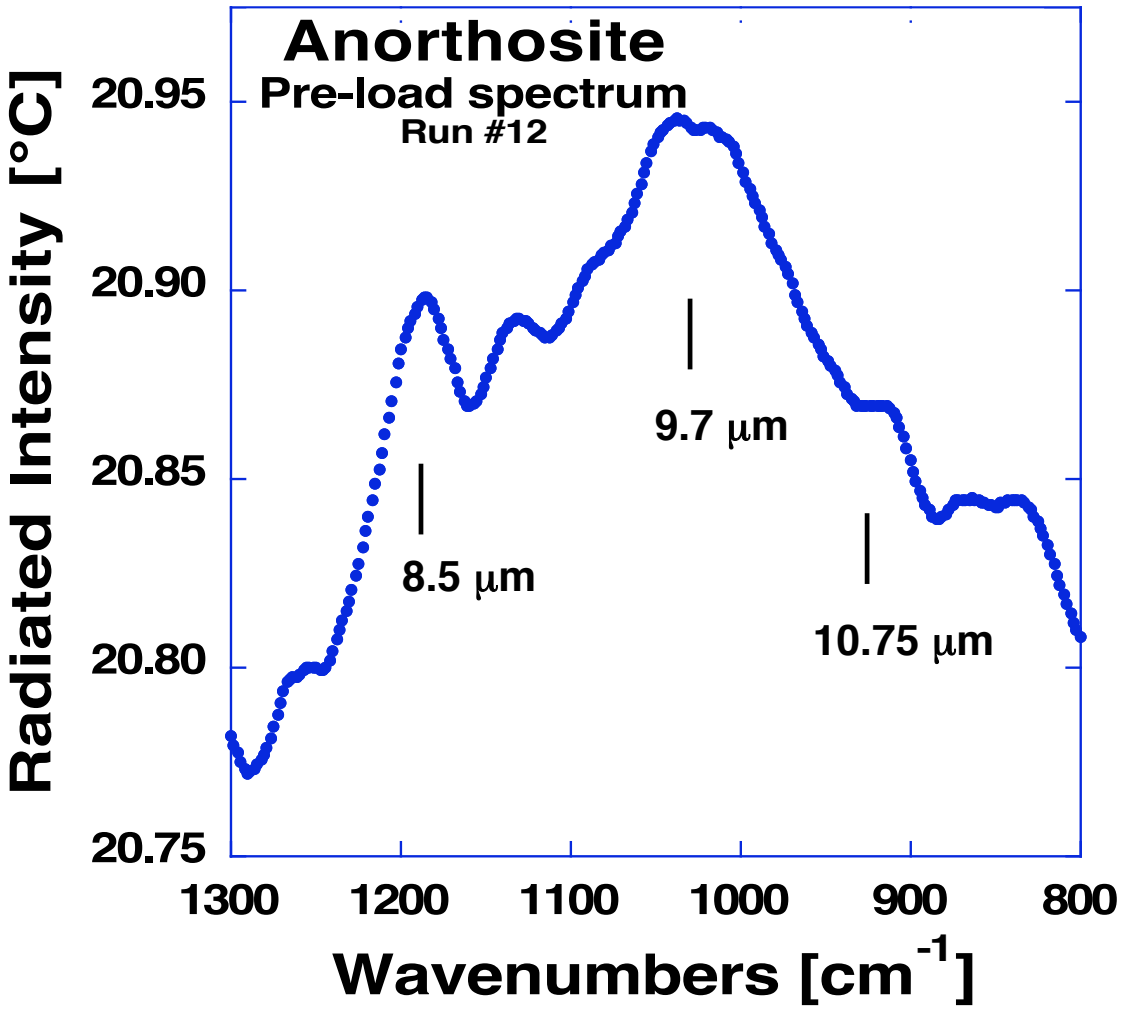

Figure 5: IR emission spectrum (average of 10 files of 25 scans each) from the flat front surface of the anorthosite block.

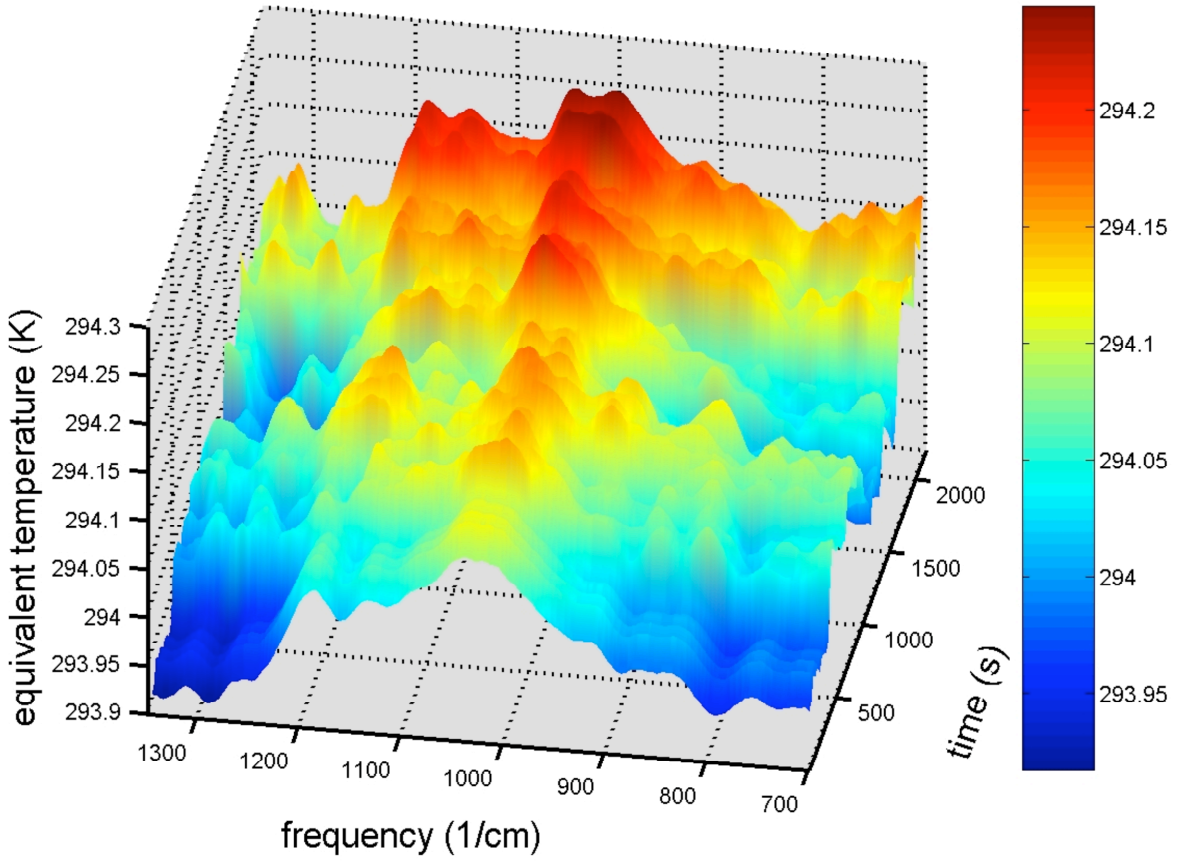

Figure 6a: 3-D plot of the intensity evolution and spectral changes of the IR emission between 8 and 12.5 μm from the front face of the anorthosite block before and during loading, plotted as a function of file numbers.

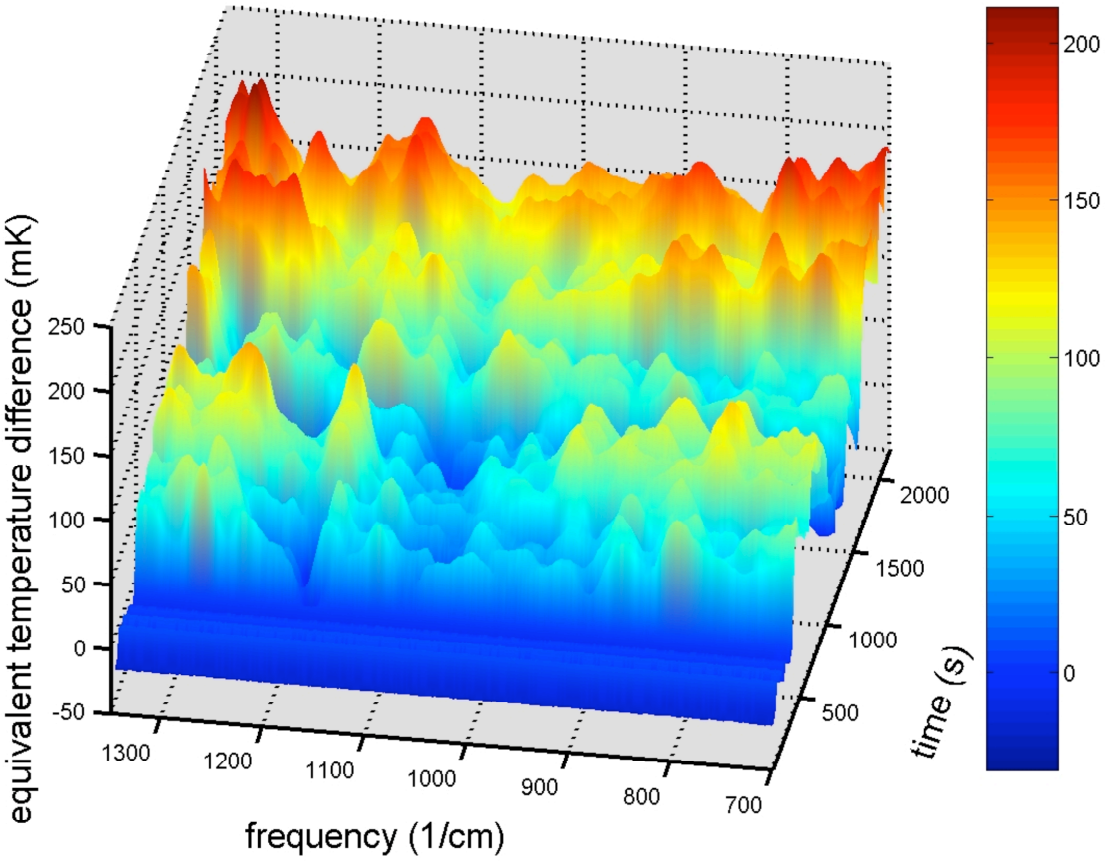

Figure 6b: Difference plot of the intensity evolution and spectral changes of the IR emission from the front face of the anorthosite block obtained by subtracting each file during loading from the average of the pre-load files.

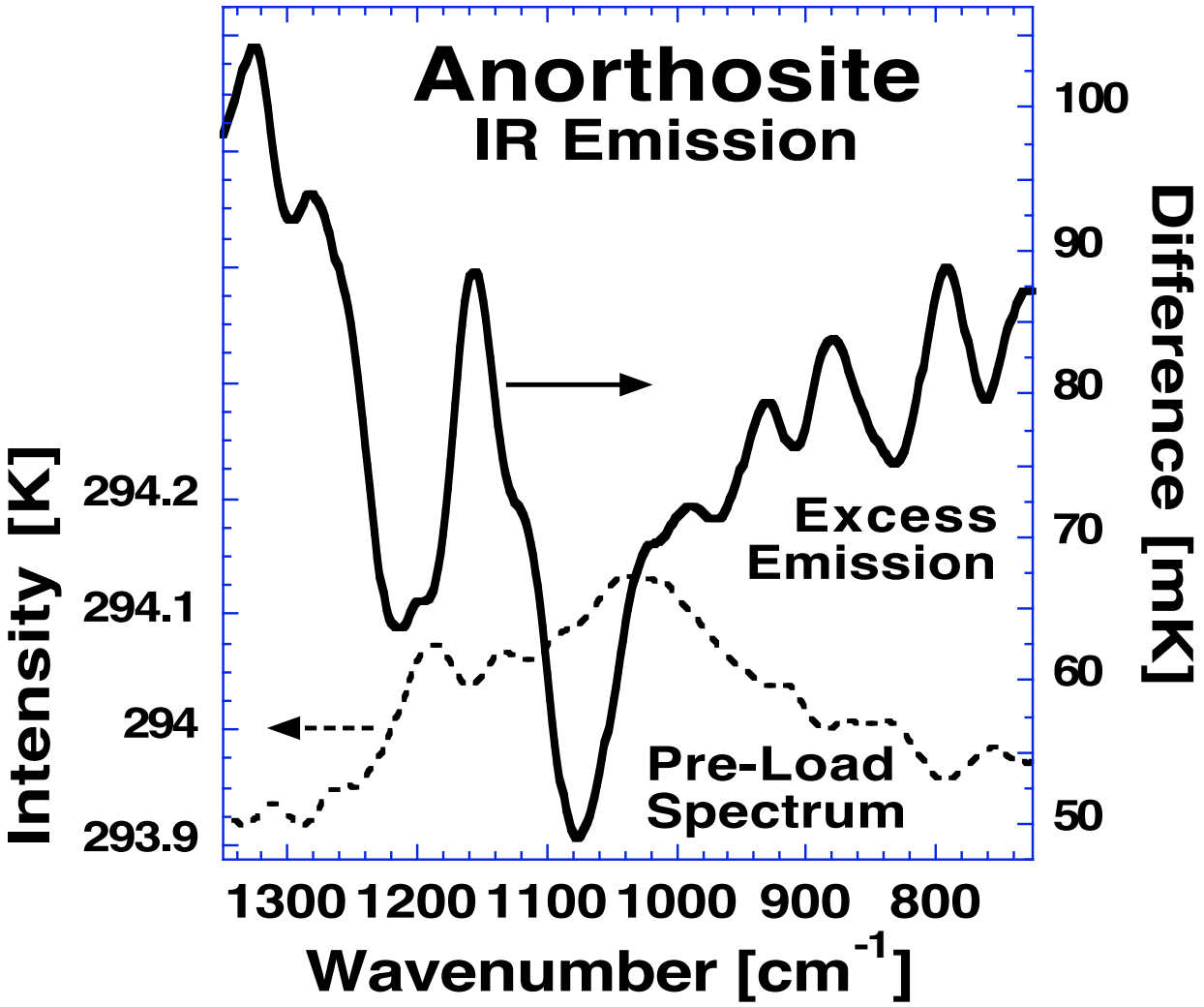

Figure 7: Total excess intensity emitted from the front face of the anorthosite block during loading (solid line) compared to the pre-load emission spectrum (dotted line).

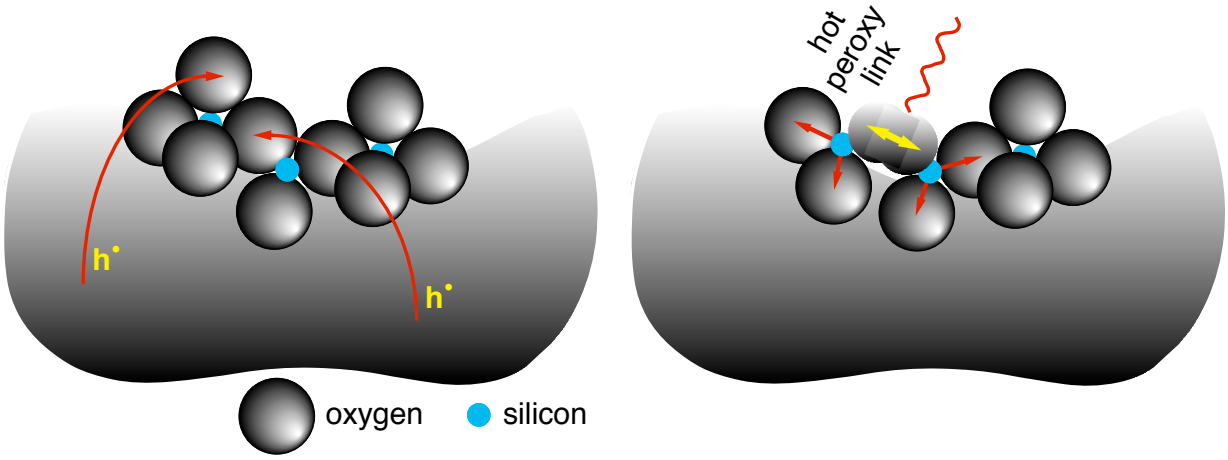

Figure 8: Schematic representation of a silica surface to illustrate the processes that take place when p-holes arrive at the surface (left). When the two p-holes recombine, the recombination energy leads to a vibrationally highly excited O-O bond, which can de-excite radiatively by emitting IR photons characteristic of transitions the energy levels of the O–O bond, and non-radiatively by channeling energy into neighboring bonds (right).

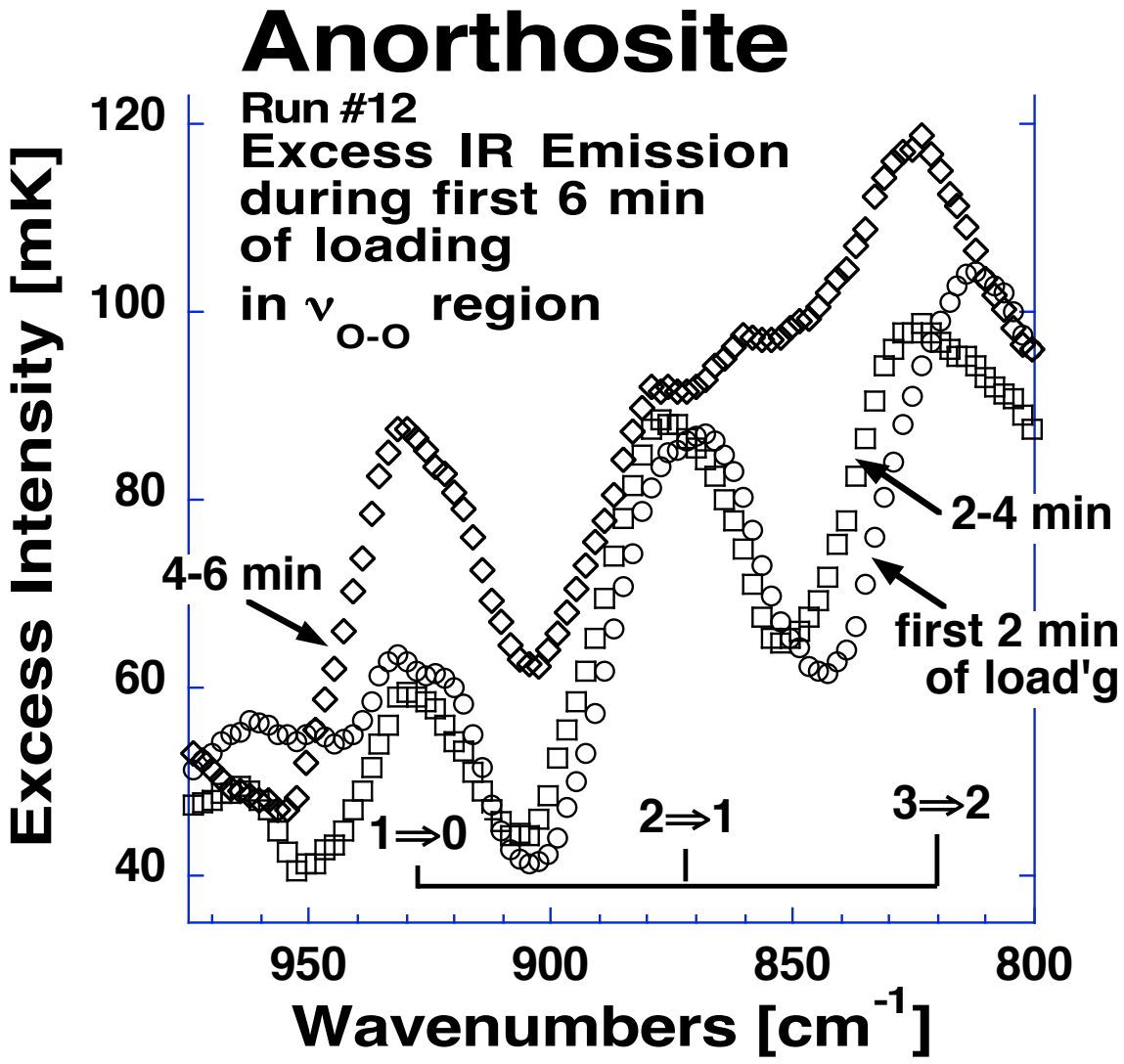

Figure 9: Evolution of the IR emission bands in the spectral window expected to contain the O-O "hot bands" and fundamental during the first 6 min of loading, broken down in 2 min intervals.